OPEN ACCESS
IOP Publishing
Superconductor Science and Technology
Supercond. Sci. Technol. **31** (2018) 025007 (14pp)
https://doi.org/10.1088/1361-6668/aa9d24

Coupling time constants of striated and copper-plated coated conductors and the potential of striation to reduce shielding-current-induced fields in pancake coils

Naoyuki Amemiya[1], Naoki Tominaga[1], Ryuki Toyomoto[1], Takuma Nishimoto[1], Yusuke Sogabe[1], Satoshi Yamano[2,3] and Hisaki Sakamoto[2]

[1] Department of Electrical Engineering, Graduate School of Engineering, Kyoto University, Kyoto-Daigaku-Katsura, Nishikyo, Kyoto 615-8510, Japan
[2] HTS Engineering Department, Furukawa Electric Co., Ltd., 6 Yawatakaigandori, Ichihara 290-8555, Japan
[3] SuperPower Inc., 450 Duane Ave., Schenectady, NY 12304, United States of America

E-mail: amemiya.naoyuki.6a@kyoto-u.ac.jp

Received 15 September 2017, revised 13 November 2017
Accepted for publication 22 November 2017
Published 9 January 2018

Abstract

The shielding-current-induced field is a serious concern for the applications of coated conductors to magnets. The striation of the coated conductor is one of the countermeasures, but it is effective only after the decay of the coupling current, which is characterised with the coupling time constant. In a non-twisted striated coated conductor, the coupling time constant is determined primarily by its length and the transverse resistance between superconductor filaments, because the coupling current could flow along its entire length. We measured and numerically calculated the frequency dependences of magnetisation losses in striated and copper-plated coated conductors with various lengths and their stacks at 77 K and determined their coupling time constants. Stacked conductors simulate the turns of a conductor wound into a pancake coil. Coupling time constants are proportional to the square of the conductor length. Stacking striated coated conductors increases the coupling time constants because the coupling currents in stacked conductors are coupled to one another magnetically to increase the mutual inductances for the coupling current paths. We carried out the numerical electromagnetic field analysis of conductors wound into pancake coils and determined their coupling time constants. They can be explained by the length dependence and mutual coupling effect observed in stacked straight conductors. Even in pancake coils with practical numbers of turns, i.e. conductor lengths, the striation is effective to reduce the shielding-current-induced fields for some dc applications.

Keywords: coated conductor, coupling time constant, magnetisation, multifilament, screening current, shielding current, striation, coupling current

(Some figures may appear in colour only in the online journal)

1. Introduction

The large magnetisation caused by shielding (screening) currents in coated conductors is a serious concern for their applications to magnets for MRI, NMR, and particle

accelerators, because it deteriorates their field qualities (shielding-current-induced field or SCIF) [1–18]. The striation of a coated conductor to divide its superconductor layer into filaments is one of the approaches to reduce the magnetisation of a coated conductor [19–45]. The striation is effective to reduce the magnetisation, i.e. SCIF, only after the decay of the coupling current flowing through the transverse resistance [39, 45]. Even if a striated coated conductor is not twisted, the coupling current could decay at a certain time constant (coupling time constant) owing to the finite length of the conductor and its finite transverse resistance [24, 25, 28]. Although the coupling time constants of non-twisted striated coated conductors wound into coils may be much larger than those of twisted multifilamentary conductors, we can wait until the coupling currents sufficiently decay after the excitation of magnets in some dc applications.

From the viewpoint of the rapid decay of coupling current, larger transverse resistance between superconductor filaments is preferable in a striated coated conductor [41, 44]. However, if it is too large or infinite, the static and transient current sharing between superconductor filaments might be prevented, and, subsequently, the tolerance against local defects of superconductor filaments and the stability of the coated conductor against time-dependent disturbance might be affected. It should be noted that the required transverse conductance for current sharing could depend on the spatial scale of local defect, spatial and time scales of disturbance, and the characteristic time of current and/or magnetic field change.

Multifilamentary coated conductors whose superconductor layers were striated using a laser and subsequently plated with copper were developed by Furukawa Electric Co., Ltd and SuperPower Inc. In these conductors, the copper plating allows current sharing between the superconductor filaments. Moreover, it covers and protects the striated edges of superconductor layers against chemical degradation. However, their small transverse resistances owing to the plated copper result in an increase in the coupling time constants.

The objective of this study is to evaluate the coupling time constants of non-twisted striated and copper-plated coated conductors of various forms: single conductors with various lengths; stacked conductors with various separations between conductors, numbers of conductors, and lengths; conductors wound into pancake coils. Using these characterisations, we aim to clarify the potential of striated and copper-plated coated conductors to reduce the SCIF in pancake coils.

The paper is organised as follows. Section 2 describes the concept of coupling currents in non-twisted striated coated conductors. In this section, first, we explain the paths of coupling currents in non-twisted striated coated conductors and the factors that determine the coupling time constants. Subsequently, we provide the Debye function for the frequency dependence of coupling loss, which is useful to obtain the coupling time constant. In section 3, we explain the method of measurement of magnetisation loss and the model for numerical electromagnetic field analysis to determine the coupling time constants. In section 4, we present the experimental results to evaluate the coupling time constants of straight striated coated conductors and their stacks and compare them with the results of numerical electromagnetic field analyses. The discussion in this section focuses on the influences of stacking and conductor length. In section 5, we estimate the coupling time constants in the striated coated conductors wound into pancake coils and discuss the potential of striation to reduce the SCIF in pancake coils. Finally, section 6 presents our conclusions.

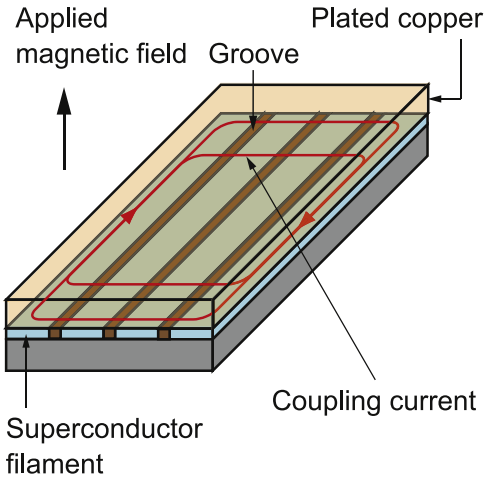

Figure 1. Coupling current in striated coated conductor.

2. Coupling currents in non-twisted striated coated conductors

2.1. Paths of coupling currents in non-twisted striated coated conductors and coupling time constants

First, we consider a straight striated coated conductor. A temporally-changing external magnetic field with a component normal to its superconductor layer can induce a coupling current, which is the shielding current flowing across the transverse resistances between superconductor filaments as shown in figure 1. The coupling time constant, which is the decay time constant of a coupling current, is determined by the self-inductance of the path of the coupling current and the resistance along the path. The resistance along the path is mainly the transverse resistance between the superconductor filaments [40, 43]. The self-inductance of the path is determined primarily by the conductor length.

Next, we consider a striated coated conductor wound into a pancake coil. When such pancake coils are stacked together, the striated coated conductor may be exposed to the magnetic field with a normal component; subsequently, this normal field component could induce a coupling current. In the case of such a striated coated conductor wound into a pancake coil, the mutual coupling between the sections of the path of the coupling current in different turns of the pancake coil might influence the inductance as shown in figure 2.

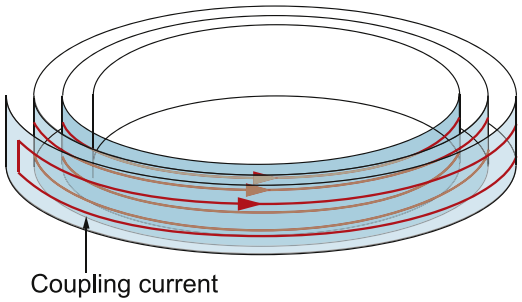

Figure 2. Mutual coupling between the sections of the coupling current path in different turns of a pancake coil.

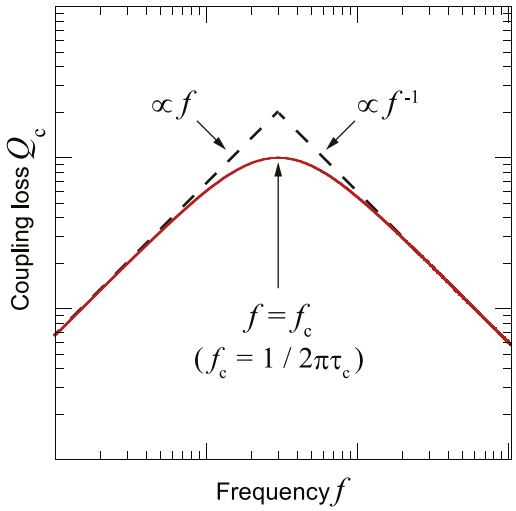

Figure 3. Debye curve of frequency dependence of coupling loss.

2.2. Debye function for the frequency dependence of coupling loss and coupling time constant

In general, the frequency dependence of the coupling loss of a multifilamentary superconductor exposed to a transverse magnetic field that changes sinusoidally is given by a Debye function as

$$Q_c = A^*\pi \cdot \mu_0 H_m^2 \frac{2\pi f\tau_c}{(2\pi f\tau_c)^2 + 1}, \quad (1)$$

where Q_c is the coupling loss per unit length per cycle, A^* is a factor determined by the geometry of the conductor, H_m is the amplitude of the applied magnetic field, f is the frequency of the applied magnetic field, and τ_c is the coupling time constant [46, 47]. Now, we define a characteristic frequency f_c as

$$f_c = 1/2\pi\tau_c \quad (2)$$

and plot the coupling loss Q_c against frequency f schematically in figure 3: Q_c is almost proportional to f when $f \ll f_c$; Q_c reaches its peak when $f = f_c$; Q_c is almost proportional to $1/f$ when $f \gg f_c$. This type of curve is called a Debye curve, which is useful to determine the coupling time constant τ_c from the magnetisation losses measured or calculated at various f. By fitting a Debye curve to the measured or calculated magnetisation losses which are dominated by coupling losses using the method of least-squares, we can determine the coupling time constant τ_c and the geometry factor A^* in equation (1).

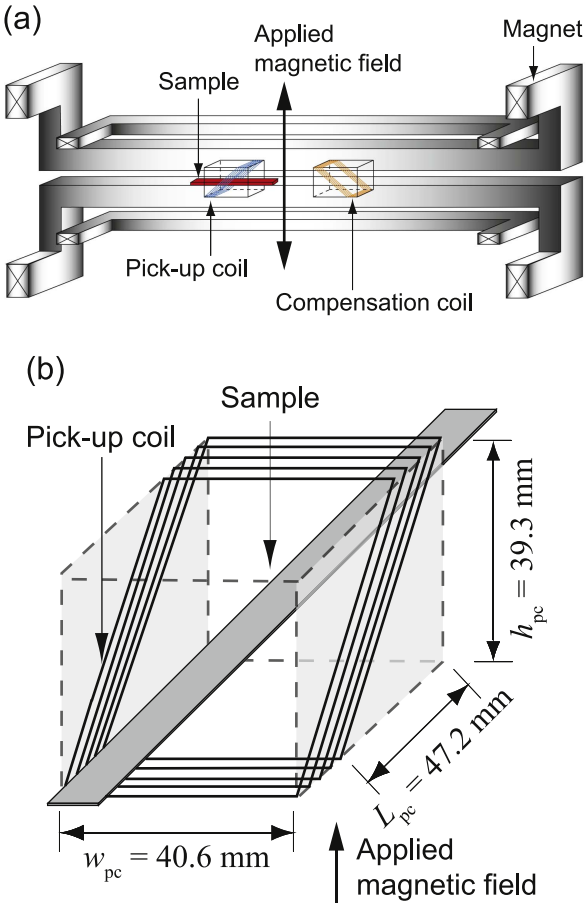

Figure 4. Schematic view of ac loss measurement system (a) and linked pick-up coil (b). (a) Reproduced from [48]. © IOP Publishing Ltd. All rights reserved. (b) © 2014 IEEE. Reprinted, with permission, from [49].

3. Experimental and theoretical methods

3.1. Method of measurement of magnetisation loss

The hysteresis loss component of magnetisation loss is proportional to H_m^3 when the magnetic field H_m is small, whereas the coupling loss component is proportional to H_m^2. Therefore, coupling losses dominate magnetisation losses when the magnetic field is small, and the frequency is near f_c. Consequently, if we apply a small magnetic field to a striated coated conductor and measure its magnetisation losses at various frequencies, we can determine τ_c by fitting equation (1) to the measured magnetisation losses.

We measured the magnetisation losses of short pieces of striated coated conductors in liquid nitrogen by using our ac loss measurement system [22, 25, 48]. Figure 4(a) shows the schematic view of the system [48, 49]. Transverse ac magnetic fields with sinusoidal waveforms were applied to a sample using a copper magnet, and the magnetisation losses were measured using a linked pick-up coil (LPC) installed around the sample conductor as shown in figure 4(b) [48]. The magnetisation loss per unit length per cycle Q_m is given as follows:

$$Q_m = C_{pc}\frac{h_{pc}H_{rms}V_{m,rms}}{N_{pc}L_{pc}f}, \quad (3)$$

Table 1. Calibration factors given by equation (4) [a] for the measured magnetisation losses of samples with various lengths.

Sample length	Calibration factor (c_l)
12.5 mm	3.70
25 mm	1.74
50 mm	1.19
100 mm	1
190 mm	1.05

[a] Equation (4): $c_l = Q_{\mathrm{Cu},100}/Q_{\mathrm{Cu},l}$.

where C_{pc} is the calibration factor of the LPC, h_{pc} is its height, N_{pc} is its number of turn, L_{pc} is the length of a turn of the LPC along the sample conductor. The calibration factor C_{pc} is determined by the cross-sectional shape of the LPC and is 2.042 for the LPC used in this study. The number of turn N_{pc} is 996, and other parameters are shown in figure 4(b). H_{rms} is the root-mean-square value of H_{m} ($\sqrt{2}\ H_{\mathrm{m}}$), and $V_{\mathrm{m,rms}}$ is the loss component of the LPC output voltage (root-mean-square value) measured using a lock-in amplifier. In all the experiments reported in this paper, $\mu_0 H_{\mathrm{m}}$ was 1 mT. As the sensitivity of the pick-up coil depends on the sample length, the LPC was calibrated. We measured the eddy current losses of copper rods of various lengths in liquid nitrogen. The ratio between the measured loss of the copper rod of length l (mm) and that of the copper rod of length 100 mm c_l given as follows

$$c_l = Q_{\mathrm{Cu},100}/Q_{\mathrm{Cu},l} \tag{4}$$

was used as the calibration factor, where $Q_{\mathrm{Cu},100}$ and $Q_{\mathrm{Cu},l}$ are the measured losses of copper rods of lengths 100 mm and l (mm), respectively. We multiplied Q_{m} calculated using equation (3) by c_l to obtain the magnetisation loss of the sample superconductor of length l (mm), because 100 mm is the standard sample length in our experimental system. The calibration factors c_l used in this study are listed in table 1.

3.2. Model for numerical electromagnetic field analysis of striated coated conductors [50, 51]

The numerical electromagnetic field analyses were carried out for a layer consisting of superconductor filaments, whose width is w_{s}, and narrow resistive strips between the superconductor filaments, whose width is w_{n}, as shown in figure 5. We refer to this layer as the analysed layer. We assumed that the thickness of the resistive strips is the same as that of the superconductor filaments t_{s}. Narrow resistive strips represented the transverse resistances between the superconductor filaments, although the components that contribute the transverse resistance and their geometries must be complicated in real striated coated conductors.

The governing equation for the numerical electromagnetic field analysis was derived from Faraday's law and Biot–Savart's law. We also applied the thin-strip approximation, where only the current density component tangential to the analysed layer is considered, and its normal component is neglected [52]. The current vector potential $\boldsymbol{T}$ is used for

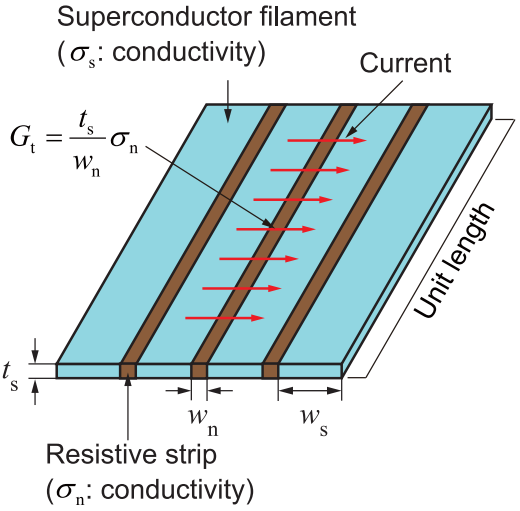

Figure 5. Thin analysed layer consisting of superconductor filaments, whose width is w_{s}, and narrow resistive strips between superconductor filaments, whose width is w_{n}, for numerical electromagnetic analyses. The thickness of the layer is t_{s}. The conductivity of the resistive strips is denoted with σ_{n}. The transverse conductance between the superconductor filaments per unit length along the coated conductor is denoted with G_{t}.

the formulation:

$$\boldsymbol{J} = \nabla \times \boldsymbol{T}. \tag{5}$$

The derived governing equation is as follows:

$$\nabla \times \left(\frac{1}{\sigma}\nabla \times \boldsymbol{n}T\right) \cdot \boldsymbol{n} + \frac{\partial}{\partial t}\left(\frac{\mu_0 t_{\mathrm{s}}}{4\pi}\int_{S'} \frac{(\nabla \times \boldsymbol{n}'T') \times \boldsymbol{r} \cdot \boldsymbol{n}}{r^3}\mathrm{d}S' + \boldsymbol{B}_{\mathrm{ext}} \cdot \boldsymbol{n}\right) = 0. \tag{6}$$

In this equation, T and T' are the current vector potential components normal to the analysed layer at the field point (the point where the field (potential) is calculated) and source point (the point where a current flows to generate the magnetic field at the field point), respectively; $\boldsymbol{n}$ and $\boldsymbol{n'}$ are the normal vectors of the analysed layer at the field point and source point, respectively; $\boldsymbol{r}$ is the vector from the source point to the field point; $\boldsymbol{B}_{\mathrm{ext}}$ is the applied external magnetic field; σ is the (equivalent) conductivity; S' is the entire area (wide face) of the analysed layer. S' consists of triangular elements, and it is flat or curved, respectively, in a straight coated conductor and a coated conductor wound into a pancake coil. Further, $\boldsymbol{n}$ and $\boldsymbol{n'}$ are identical and constant in a non-twisted straight coated conductor, but they are different and vary in a coated conductor wound into a pancake coil. Equation (6) was discretized, and the derived system of equations were solved to obtain the time-dependent spatial distribution of T. A typical number of unknown valuables T is around 30 000. The details of the model are given in [50, 51].

For the sake of simplicity, we assumed that the magnetic field dependence of the critical current density J_{c} was solely determined by the magnetic field component normal to the superconductor layer $B_{\perp}$. The superconducting property is

Table 2. Specifications of coated conductors used in experiments and numerical electromagnetic field analyses.

Geometry	4 mm wide, four-filament coated conductor Single coated conductor or stacked coated conductors	2 mm wide, two-filament coated conductor Pancake coil
Width of coated conductor	4 mm	2 mm
Thickness of coated conductor (t_{cc})	98 μm (measured value)	100 μm
Thickness of plated copper (t_{Cu})	20 μm	—
Thickness of superconductor layer (t_s)	1.7 μm	1.7 μm
Number of superconductor filaments	4	2
Critical current before striation	135.8 A	—
Critical current after striation	130 A	—
E_0 of power law E–J characteristic given by equation (7)[a]	1×10^{-4} V m^{-1}	1×10^{-4} V m^{-1}
n of power law E–J characteristic given by equation (7)[a]	30	30
Critical current density at zero field (J_{c0})	2.10×10^{10} A m^{-1}	2.10×10^{10} A m^{-1}
Constant B_0 in Kim's model given by equation (9)[b]	200 mT	200 mT
Width of groove between superconductor filaments (w_g)[c]	57 μm	—
Width of resistive strip between superconductor filaments in numerical electromagnetic field analyses (w_n)[d]	50 μm	50 μm
Transverse conductance between superconductor filaments per unit length along the coated conductor ($G_{t,e}$)[e]	3.47×10^{7} Ω^{-1} m^{-1}	3.47×10^{7} Ω^{-1} m^{-1}
Conductivity of narrow resistive strip in the model for numerical electromagnetic field analyses (σ_n)[e]	1.02×10^{9} Ω^{-1} m^{-1}	1.02×10^{9} Ω^{-1} m^{-1}

[a] Equation (7): $E = E_0(J/J_c(B_\perp))^n$.
[b] Equation (9): $J_c(B_\perp) = J_{c0}[B_0/(B_0 + |B_\perp|)]$.
[c] w_g is determined in section 4.1.
[d] w_n is a rounded value of w_g.
[e] $G_{t,e}$ and σ_n are determined in section 4.2.

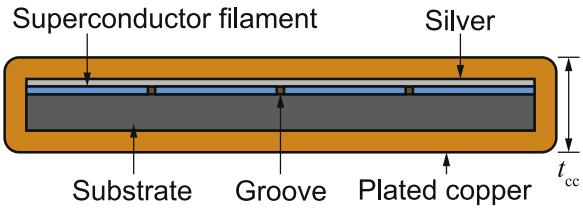

Figure 6. Schematic cross section of striated coated conductor. The thickness of the coated conductor is t_{cc}.

given by the power law E–J characteristic [53, 54]:

$$E = E_0\left(\frac{J}{J_c(B_\perp)}\right)^n, \tag{7}$$

where E_0 is 10^{-4} V m^{-1}. Subsequently, the equivalent conductivity of the superconductor $\sigma_s(\boldsymbol{nT})$ was derived as

$$\sigma_s(\boldsymbol{nT}) = \frac{J}{E} = \frac{J_c}{E_0}\left(\frac{J_c}{J}\right)^{n-1} = \frac{J_c}{E_0}\left(\frac{J_c}{|\nabla \times \boldsymbol{nT}|}\right)^{n-1}. \tag{8}$$

In order to reduce the computation time required for iterative calculations, we set the maximum equivalent conductivity as 10^{300} Ω^{-1} m^{-1}. The magnetic field dependence of the local critical current density is given by Kim's model as

$$J_c(B_\perp) = J_{c0}\frac{B_0}{B_0 + |B_\perp|} \tag{9}$$

where J_{c0} is the critical current density at zero magnetic field and B_0 is a constant [55].

The conductivity of the resistive strips σ_n representing the transverse resistances between the superconductor filaments was set as a constant value for an analysis.

After calculating $\boldsymbol{T}$, we can obtain $\boldsymbol{J}$, i.e. the current distribution, by using equation (5). Using the following expression, we can calculate the magnetisation loss per unit length per cycle:

$$Q_m = \frac{t_s}{l}\int_{1/f}\int_{S'} E \cdot J \mathrm{d}S'\mathrm{d}t, \tag{10}$$

where l is the conductor length. In all the numerical electromagnetic field analyses reported in this paper, sinusoidal transverse magnetic fields with $\mu_0 H_m$ of 1 mT were applied to the conductors.

4. Coupling time constants of straight striated coated conductors and their stacks

4.1. 4 mm wide, four-filament coated conductor

The specifications of the striated coated conductor used in the experiments and numerical electromagnetic field analyses are listed in table 2, and its schematic cross section is shown in figure 6, respectively. Its superconductor layer with silver protective layer was cut into four filaments using a laser, covered with additional silver layer and subsequently plated with copper. Grooves between superconductor filaments cut by laser might be filled with residual materials melted by laser, silver, and copper. Eventually, their superconductor filaments were connected electrically mainly through the plated copper. From the difference between the critical currents before and after the striation (laser cutting), we simply assumed that 4.27% of the superconductor layer was lost; the estimated width of each striated groove between the superconductor filaments w_g is 57 μm. In the numerical electromagnetic field analyses, the width of resistive strip w_n was set as the rounded value of 50 μm. The value of conductivity of the resistive strip σ_n in table 2 will be determined in section 4.2. Measurements of magnetisation loss to determine the coupling time constants and numerical electromagnetic field analyses were conducted using single straight conductors and stacked straight conductors.

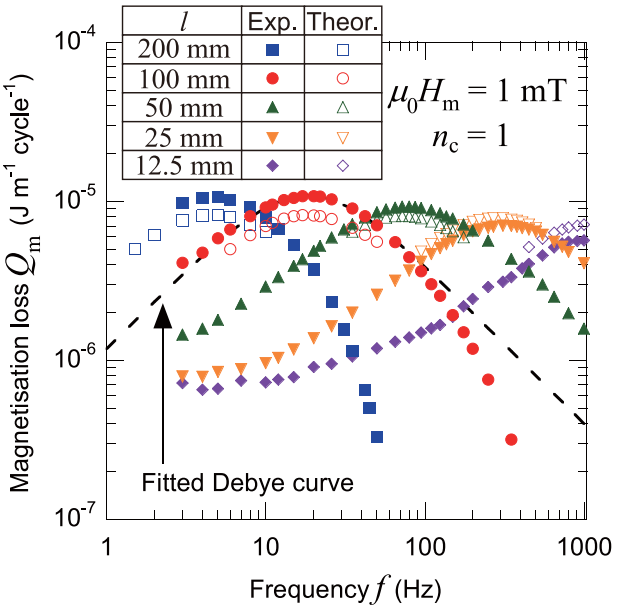

Figure 7. Magnetisation loss per unit length per cycle Q_m of single conductors with various conductor lengths l versus frequency f when the amplitude of the applied normal magnetic field $\mu_0 H_m$ is 1 mT. Closed symbols denote measured values, and open symbols denote theoretical values obtained from numerical electromagnetic field analyses where σ_n is 1.02×10^9 Ω^{-1} m^{-1}. The broken line denotes the Debye curve with $\tau_c = 8.66$ ms fitted to the measured Q_m for $l = 100$ mm using the method of least-squares.

4.2. Coupling time constants of single striated coated conductors of various lengths, transverse conductance between superconductor filaments, and current distributions

We measured the magnetisation losses of single straight striated coated conductors. In figure 7, the measured magnetisation losses Q_m of single conductors of various lengths l are plotted against frequency f with closed symbols. The broken line denotes the Debye curve with $\tau_c = 8.66$ ms fitted to the measured magnetisation losses for $l = 100$ mm using the method of least-squares. The frequency f_c, which provides the peak of the Q_m–f plot, decreases with an increase in conductor length. By fitting equation (1) to the measured Q_m–f plots, the coupling time constants τ_c for various conductor lengths are determined and plotted against conductor length with closed symbols in figure 8. These experimentally determined coupling time constants τ_c are almost proportional to the square of conductor length l, and the following

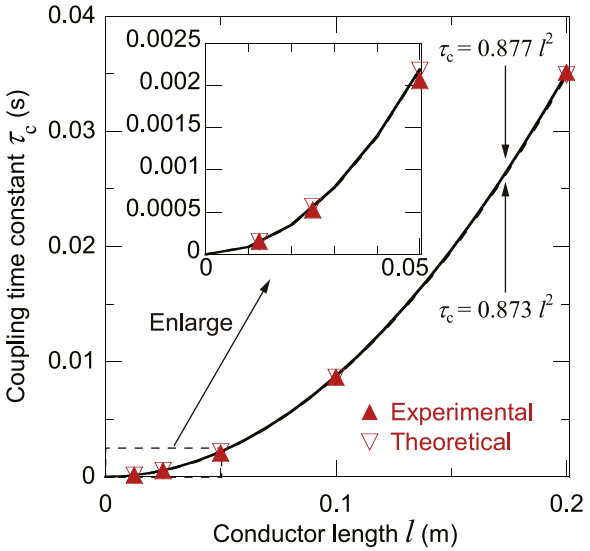

Figure 8. Coupling time constant τ_c versus conductor length l for single conductors. Closed symbols denote experimentally determined values, and open symbols denote theoretically determined values obtained from numerical electromagnetic field analyses where σ_n is $1.02 \times 10^9\ \Omega^{-1}\ m^{-1}$. Equation (11) was fitted to the experimentally determined values and the theoretically determined values by using the method of least-squares in order to determine the factors of proportionality for τ_c shown in the figure. The fitted curves for the experimentally determined values and those for the theoretically determined values are shown with the solid and broken lines, respectively.

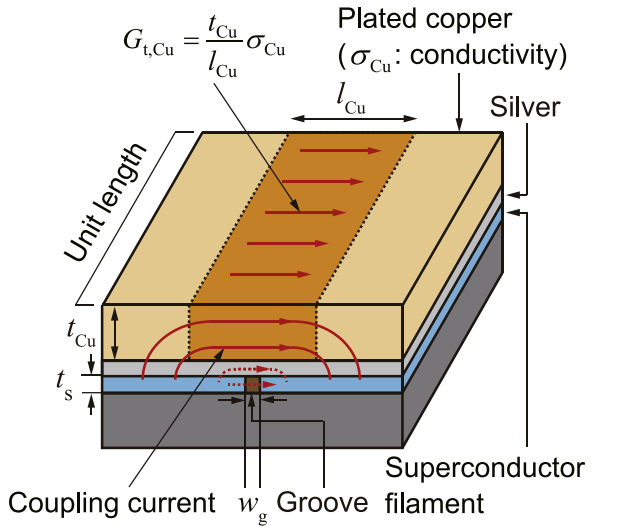

Figure 9. Model of transverse conductance (resistance) between superconductor filaments dominated by the copper layer plated over the superconductor layer. We assume that the current flows uniformly along the copper layer whose thickness and effective length contributing the transverse conductance (resistance) are t_{Cu} and l_{Cu}, respectively. The conductivity of the copper is denoted with σ_{Cu}. The transverse conductance between the superconductor filaments per unit length along the coated conductor is denoted with $G_{t,Cu}$.

expression can be fitted to them by using the method of least-squares:

$$\tau_c = al^2, \tag{11}$$

where the units of τ_c and l are second and metre, respectively. The factor of proportionality a determined by the fitting is $0.877\ s\ m^{-2}$. The fitted curve is shown with a solid line in the figure.

For the single conductor with $l = 100$ mm, we varied conductivity of the resistive strip σ_n and carried out the numerical electromagnetic field analyses in order to determine the value of σ_n with which the measured Q_m–f plot can be reproduced. The value of σ_n obtained is $1.02 \times 10^9\ \Omega^{-1}\ m^{-1}$, and according to this value, $\tau_c = 8.66$ ms ($f_c = 18.4$ Hz). This value of σ_n is used in the numerical electromagnetic field analyses in the following part of this paper. The transverse conductance between the superconductor filaments per unit length along the coated conductor G_t shown in figure 5 can be calculated as follows:

$$G_t = \frac{t_s}{w_n}\sigma_n. \tag{12}$$

When σ_n is $1.02 \times 10^9\ \Omega^{-1}\ m^{-1}$, G_t is $3.47 \times 10^7\ \Omega^{-1}\ m^{-1}$. This G_t determined by the experiments and numerical electromagnetic field analyses is denoted as $G_{t,e}$ in the following discussion.

The transverse conductance between the superconductor filaments could be the parallel circuits consisting of the 20 μm thick copper layer plated over the superconductor layer, a much thinner additional silver layer, and materials in the 1.7 μm thick groove (copper, silver, and melted residuals) as shown in figure 9. It is reasonable to assume that the copper layer could dominate the transverse conductance, because it is much thicker and is more conductive than others. We estimate the transverse conductance based on this assumption. We assume that the current flows uniformly along the copper layer whose thickness and effective length that contribute the transverse conductance (resistance) are t_{Cu} and l_{Cu}, respectively, as shown in figure 9. The transverse conductance between the superconductor filaments per unit length along the coated conductor $G_{t,Cu}$ is given as follows:

$$G_{t,Cu} = \frac{t_{Cu}}{l_{Cu}}\sigma_{Cu} \tag{13}$$

where σ_{Cu} is the conductivity of copper, which is $5 \times 10^8\ \Omega^{-1}\ m^{-1}$ at 77 K and t_{Cu} is 20 μm. In figure 10, the calculated $G_{t,Cu}$ is plotted against effective copper length l_{Cu} and is compared with $G_{t,e}$. When the effective copper length is w_g (57 μm), $G_{t,Cu}$ is much larger than $G_{t,e}$. This is expected, because w_g should be the minimum path of the transverse current flowing through the copper layer. If the effective copper length is assumed to be approximately 300 μm, $G_{t,Cu}$ becomes equal to $G_{t,e}$. There are advantages and a drawback in the transverse resistance (conductance) dominated by the plated copper. The thickness of the plated copper can be uniform along a conductor and controllable. The consequent uniformity and controllability of the transverse resistance could be advantages. We can increase the transverse resistance, i.e. decrease the coupling time constant, by decreasing the copper thickness or by using a copper alloy instead of copper. A drawback is decreasing transverse resistance with

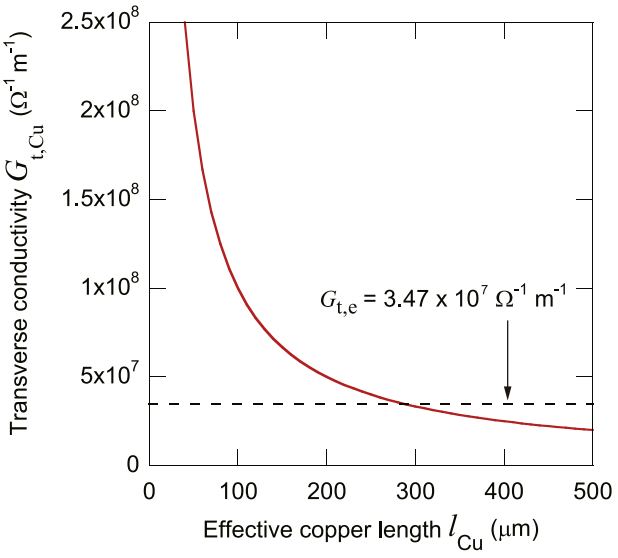

Figure 10. Transverse conductivity $G_{t,Cu}$ calculated as $(t_{Cu}/l_{Cu})\sigma_{Cu}$ where σ_{Cu} is the conductivity of copper, which is $5 \times 10^8\ \Omega^{-1}\ m^{-1}$ at 77 K and t_{Cu} is 20 μm. $G_{t,e}$ is the transverse conductance determined by experiments and numerical electromagnetic field analyses.

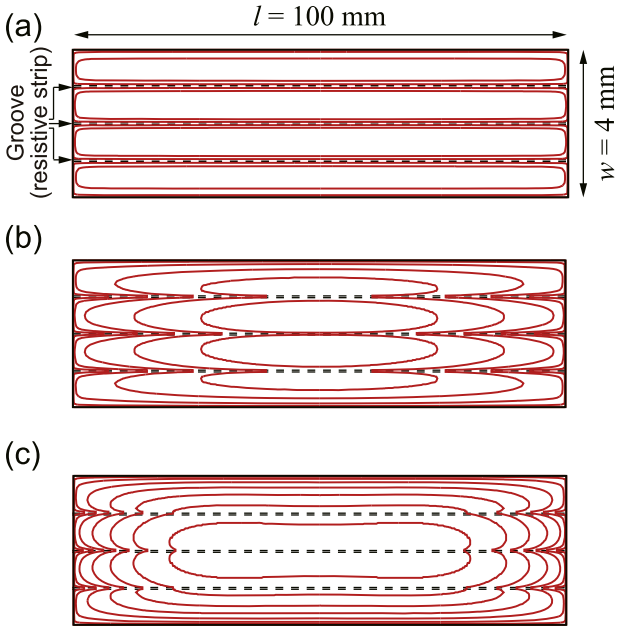

Figure 11. Calculated current lines on the striated coated conductor ($l = 100$ mm) at the peak of the applied sinusoidal magnetic field: (a) $f = f_c/10$, (b) $f = f_c$, and (c) $f = 10 f_c$ where σ_n is $1.02 \times 10^9\ \Omega^{-1}\ m^{-1}$ and, then, $f_c = 18.4$ Hz. Figures are expanded laterally to improve legibility.

decreasing temperature. Consequently, the coupling time constant could be inversely proportional to the temperature-dependent resistivity of copper. It should be noted that the interlayer resistances between copper, silver, and superconductor layers can reduce the transverse conductance.

We carried out the numerical electromagnetic field analyses at various frequencies for single conductors of various conductor lengths. In figure 7, the calculated magnetisation losses are plotted with open symbols. In this figure, the calculated losses are reasonably consistent with the measured ones. In the electromagnetic field analyses, the coupling currents are confined in the layer whose thickness is t_s shown in figure 5, whereas the coupling currents in the experiments expand in the copper layer on the superconductor layer as shown in figure 9. The difference in the coupling current paths may cause the difference between the measured and calculated losses. By fitting equation (1) to the calculated Q_m–f plots, the coupling time constants are determined and are plotted against conductor length with open symbols in figure 8. These theoretically determined coupling time constants are also almost proportional to the square of conductor length, and equation (11) can be fitted to them with a of $0.873\ s\ m^{-2}$ by using the method of least-squares. The fitted curve is shown with a broken line in the figure. This theoretically determined a of $0.873\ s\ m^{-2}$ is 99.5% of the experimentally determined a of $0.877\ s\ m^{-2}$.

In figures 11(a)–(c), the calculated current lines on the striated coated conductor ($l = 100$ mm) at the peak of the applied sinusoidal magnetic field are shown for $f = f_c/10$, f_c, and $10f_c$ where f_c is = 18.4 Hz. The corresponding lateral current distributions at the centre of the conductor are shown in figures 12(a)–(c). The superconductor filaments are decoupled completely at $f_c/10$, coupled partially at f_c, and coupled mostly at $10f_c$.

4.3. Influence of stacking striated coated conductors on coupling time constants

We measured the magnetisation losses of the stacks of straight striated coated conductors. Stacked conductors simulate the turns of a conductor wound into a pancake coil. We varied the number of stacked conductors n_c and the separation between conductors d, whereas conductor length l was fixed at 50 mm. When we stacked the conductors, polyimide sheets and/or GFRP sheets were placed to maintain the separation between conductors, and a GFRP sample holder was used to reduce the lateral misalignments of stacked conductors in most of the experiments.

In figure 13, the measured magnetisation losses of stacked conductors with various numbers of stacked conductors n_c and the separation between conductors $d = 0.1$ mm are plotted against frequency f with closed symbols. The characteristic frequency f_c, which gives the peak of a Q_m–f plot, decreases with increasing number of stacked conductors. In figure 14, the measured magnetisation losses of stacked conductors with various separations between conductors d and number of stacked conductor $n_c = 8$ are plotted against frequency f with closed symbols. The characteristic frequency increases with increasing separation between conductors. In these figures, we can observe the influence of stacking on the Q_m–f plots. Further, Q_m–f measurements were carried out for various combinations of n_c and d. We determine the values of coupling time constant for various combinations of n_c and d by fitting equation (1) to the measured Q_m–f plots. In figure 15, the experimentally determined coupling time constants are plotted against number of stacked conductors with closed symbols where d = 0.05–1 mm. The coupling time

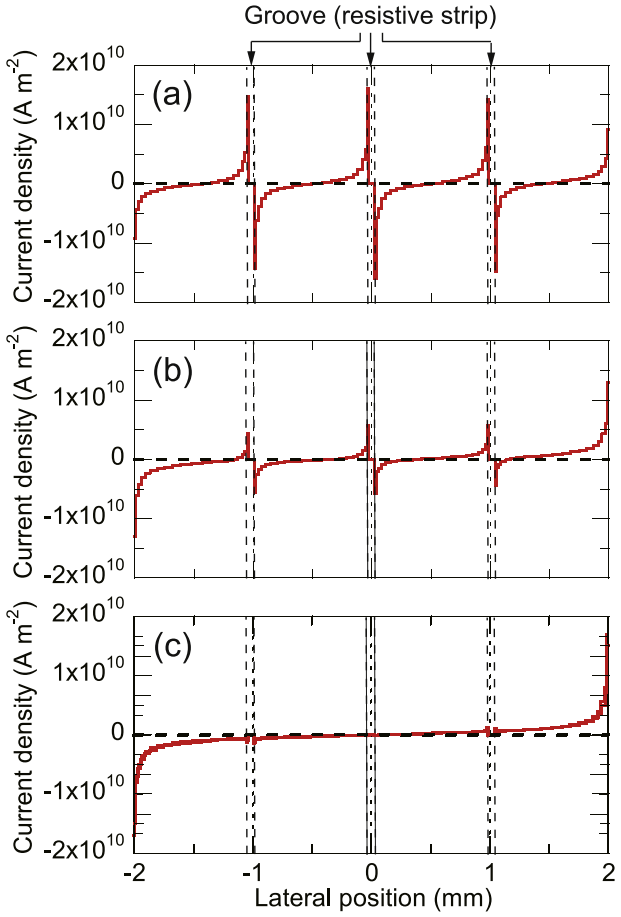

Figure 12. Calculated lateral current distributions at the centre of the striated coated conductor ($l = 100$ mm) at the peak of the applied sinusoidal magnetic field: (a) $f = f_c/10$, (b) $f = f_c$, and (c) $f = 10 f_c$ where σ_n is 1.02×10^9 Ω^{-1} m^{-1} and then, $f_c = 18.4$ Hz.

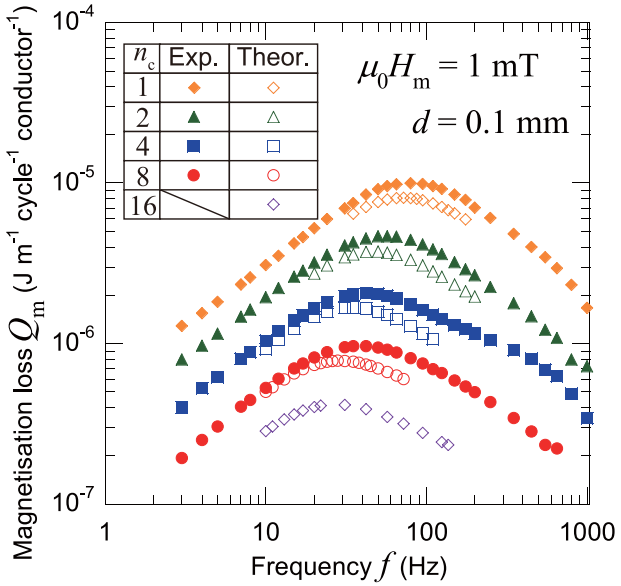

Figure 13. Magnetisation loss per unit length per cycle Q_m of stacked conductors with $d = 0.1$ mm and $l = 50$ mm versus frequency f when the amplitude of the applied normal magnetic field $\mu_0 H_m$ is 1 mT. Closed symbols denote measured values, and open symbols denote theoretical values obtained from numerical electromagnetic field analyses where σ_n is 1.02×10^9 Ω^{-1} m^{-1}.

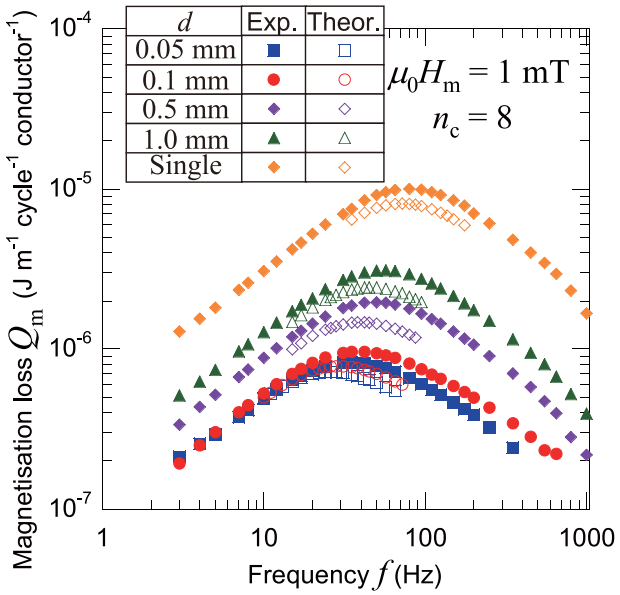

Figure 14. Magnetisation loss per unit length per cycle Q_m of stacked conductors with $n_c = 8$ and $l = 50$ mm versus frequency f when the amplitude of the applied normal magnetic field $\mu_0 H_m$ is 1 mT. Closed symbols denote measured values, and open symbols denote theoretical values obtained from numerical electromagnetic field analyses where σ_n is 1.02×10^9 Ω^{-1} m^{-1}.

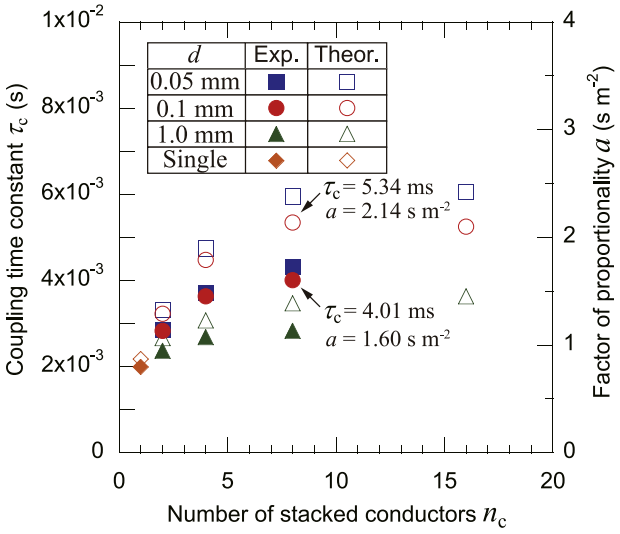

Figure 15. Coupling time constant τ_c and factor of proportionality a of equation (11) versus number of stacked conductors n_c where $d = 0.05$–1 mm and $l = 50$ mm. The value of a was calculated directly from each τ_c by using equation (11); each point represents τ_c in the left vertical axis and a in the right vertical axis. Closed symbols denote experimentally determined values, and open symbols denote theoretically determined values obtained from numerical electromagnetic field analyses where σ_n is 1.02×10^9 Ω^{-1} m^{-1}.

constants increase with increasing number of stacked conductors. Figure 16 schematically shows the coupling currents in stacked conductors. The mutual coupling of the coupling currents in different conductors could increase coupling time constants. In figure 17, the experimentally determined coupling time constants are plotted against separation between conductors with closed symbols where n_c = 1–8. The

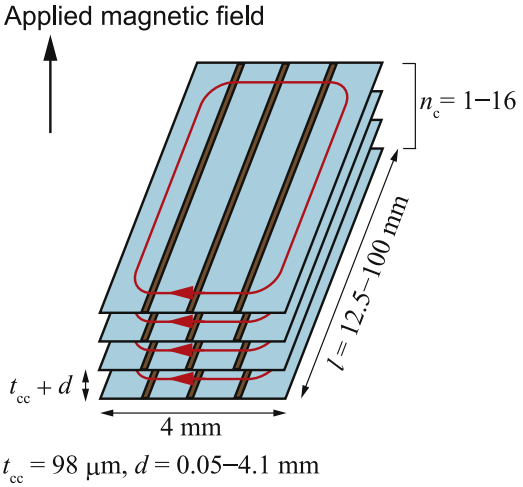

Figure 16. Coupling currents in stacked striated coated conductors. The mutual coupling of the coupling currents in different conductors could result in an increase in coupling time constant. The separation between superconductor layers is $t_{cc} + d$, where t_{cc} and d are the thickness of coated conductor and the separation between coated conductors, respectively.

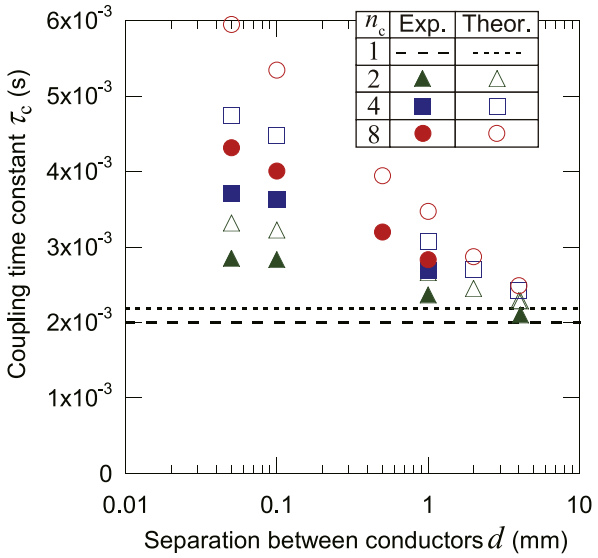

Figure 17. Coupling time constant τ_c versus separation between conductors d where n_c = 1–8 and l = 50 mm. Closed symbols denote experimentally determined values, and open symbols denote theoretically determined values obtained from numerical electromagnetic field analyses where σ_n is 1.02 × 10^9 Ω^{-1} m^{-1}.

coupling time constants decrease with increasing separation between conductors. When d = 4.1 mm, the coupling time constant for n_c = 2 falls to 2 ms, which is almost equal to the coupling time constant of a single conductor. With increasing separation between conductors, mutual coupling between the coupling currents in different conductors could be reduced. This could be the reason for the decrease in coupling time constant with increasing separation between conductors. In figure 15, the increasing coupling time constant saturates at larger number of stacked conductors. This saturation is more remarkable for larger separation between conductors. As shown in figure 17, the coupling currents in distant

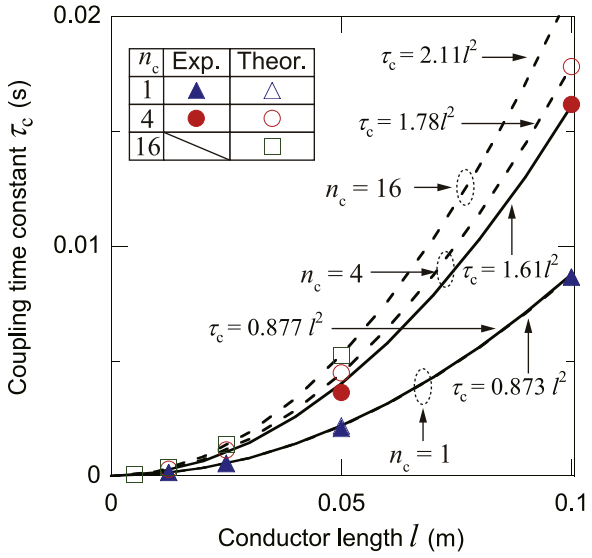

Figure 18. Coupling time constant τ_c versus conductor length l for stacked conductors with various n_c where d = 0.1 mm. Closed symbols denote experimentally determined values (n_c = 1 and 4; l = 12.5 mm, 25 mm, 50 mm, and 100 mm), and open symbols denote theoretically determined values (n_c = 1, 4 and 16; l = 5 mm, 12.5 mm, 25 mm, 50 mm, and 100 mm) obtained from numerical electromagnetic field analyses where σ_n is 1.02 × 10^9 Ω^{-1} m^{-1}. Equation (11) was fitted to the experimentally determined values and the theoretically determined values by using the method of least-squares in order to determine the factors of proportionality for τ_c shown in the figure. The fitted curves for the experimentally determined values and those for the theoretically determined values are shown with the solid and broken lines, respectively.

conductors are less coupled. This could be the reason for the saturation, because some of the other conductors are located more distantly in a stack with large number of stacked conductors and/or separation between conductors.

We carried out the numerical electromagnetic field analyses at various frequencies for stacked conductors with various n_c and d. In figures 13 and 14, the calculated magnetisation losses are plotted with open symbols. We also determine coupling time constants for various combinations of number of stacked conductors and separation between conductors by fitting equation (1) to the calculated Q_m–f plots. These theoretically determined coupling time constants are plotted with open symbols in figures 15 and 17. In figure 15, the theoretically determined coupling time constants and the experimentally determined coupling time constants saturate at larger number of stacked conductors although the former is larger than the latter. As mentioned in section 4.2, the difference between the coupling current paths may cause the difference between the experimentally determined and theoretically determined coupling time constants.

4.4. Coupling time constants of stacked striated coated conductors of various lengths

In figure 18, the experimentally determined and theoretically determined coupling time constants are plotted against conductor length with closed circles and open circles, respectively, for n_c = 4 and d = 0.1 mm. The corresponding values

for single conductors ($n_c = 1$) shown in figure 8 are replotted with triangles. For $n_c = 16$ and $d = 0.1$ mm, the theoretically determined coupling time constants are plotted with open squares. The experimentally determined or theoretically determined coupling time constants of stacked striated coated conductors for each n_c are proportional to l^2. Equation (11) was fitted to them by using the method of least-squares in order to determine the factor of proportionality a, and the determined values of a are shown in the figure. The fitted curves for the experimentally determined and theoretically determined coupling time constants are shown with the solid and broken lines, respectively.

Assuming that any value of coupling time constant is proportional to the square of conductor length, the factor of proportionality a of equation (11) can be determined directly from the coupling time constant for a single conductor length. In figure 15, the value of a was calculated directly from each coupling time constant by using equation (11); each point in the figure represents coupling time constant in the left vertical axis and the factor of proportionality in the right vertical axis. Similar to coupling time constant, the factor of proportionality saturates at larger number of stacked conductors.

The results in section 4 can be summarised as follows.

(1) The coupling time constant of stacked conductors and that of a single conductor are proportional to the square of the conductor length.
(2) The coupling time constant increases by stacking conductors.
(3) The increase in the coupling time constant by stacking saturates with the increase in the number of conductors. It saturates at a smaller number of conductors when the separation between conductors is larger.

5. Coupling time constants of striated coated conductors wound into pancake coils

5.1. Numerical electromagnetic field analyses of 2 mm wide, two-filament coated conductors wound into pancake coils

We studied the coupling time constants of the striated coated conductors wound into pancake coils using numerical electromagnetic field analyses. In order to reduce the computation loads, we used a 2 mm wide, two-filament coated conductor. Comprehensive analyses were performed for the followings:

(1) stacked straight conductors with various numbers of stacked conductors;
(2) conductors wound into pancake coils with various numbers of turns n_t;
(3) single straight conductors whose lengths l are identical to those of (2).

The detailed specifications of the 2 mm wide, two-filament coated conductor are listed in table 2, and those of the pancake coils are listed in table 3. In the model, the actual spiral geometry of the conductor in a pancake coil as shown in figure 19 was considered. A sinusoidal magnetic field whose amplitude was 1 mT was applied normally and uniformly to the striated coated conductors with $\sigma_n = 1.02 \times 10^9$ Ω^{-1} m^{-1} and $w_n = 50$ μm.

Table 3. Specifications of pancake coils wound with 2 mm wide, two-filament coated conductor used in numerical electromagnetic field analyses.

Inner radius (R_{in})	25 mm
Outer radius (R_{out})	25.2/25.4/25.8/26.6/28.2 mm
Number of turns	1/2/4/8/16
Turn separation	0.1 mm
Conductor length	158/317/638/1297/2674 mm

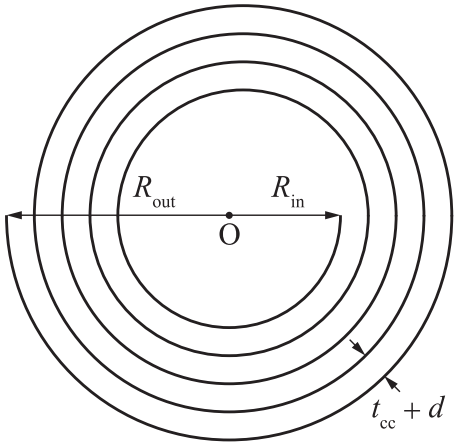

Figure 19. Spiral geometry of coated conductor wound into pancake coil. The inner and outer radii of a pancake coil are R_{in} and R_{out}, respectively. The separation between superconductor layers is $t_{cc} + d$, where t_{cc} and d are the thickness of coated conductor and the separation between coated conductors, respectively.

In preparation for the analyses of pancake coils, we investigate the stacked 2 mm wide, two-filament coated conductors. In figure 20, coupling time constant τ_c as well as the factor of proportionality a of equation (11), which were calculated directly from each coupling time constant, are plotted against number of stacked conductors where $d = 0.1$ mm and $l = 50$ mm. Because of mutual coupling, the factor of proportionality a of equation (11) increases with increasing number of stacked conductors n_c, but it saturates around $n_c = 16$. For this 2 mm wide, two-filament coated conductor, $a = 1.42$ s m^{-2} when $n_c = 1$, and 2.75 s m^{-2} when $n_c = 16$. We will use these two values in the discussion below.

Then, we compare the coupling time constants τ_c of the conductors wound into pancake coils and those of the reference single straight conductors whose lengths are identical to the conductors wound into pancake coils. In figure 21, the calculated magnetisation loss Q_m of conductors wound into pancake coils with various numbers of turns, i.e. conductor lengths, and those of single straight conductors with the corresponding conductor lengths are plotted against frequency with closed symbols and open symbols, respectively. We determined coupling time constants by fitting equation (1)

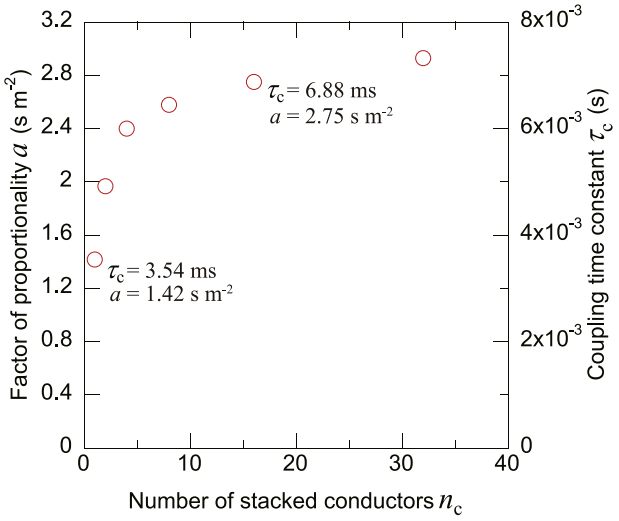

Figure 20. Calculated factor of proportionality a of equation (11) and coupling time constant τ_c versus number of stacked 2 mm wide, two-filament conductors n_c where $d = 0.1$ mm and $l = 50$ mm. The value of a was calculated directly from each τ_c by using equation (11).

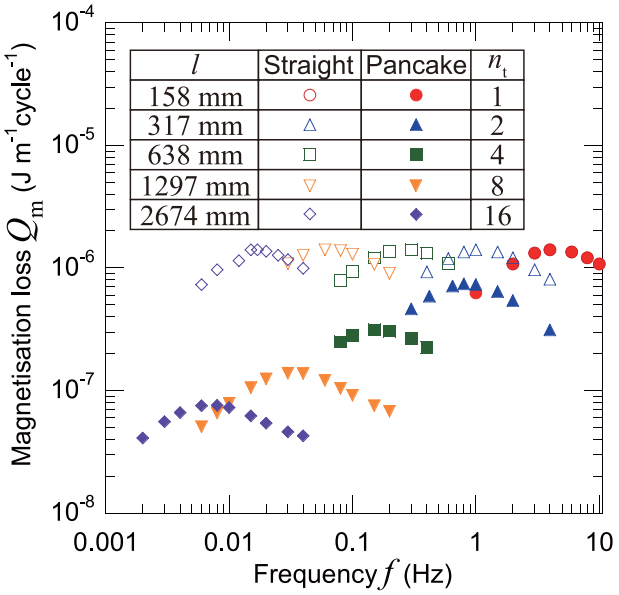

Figure 21. Calculated magnetisation loss per unit length per cycle Q_m of conductors wound into pancake coils with various n_t, i.e. l, (closed symbols) and those of single straight conductors with corresponding l (open symbols) versus frequency f when the amplitude of the applied normal magnetic field $\mu_0 H_m$ is 1 mT.

to the calculated Q_m–f plots. In figure 22, the determined coupling time constants of the conductors wound into pancake coils and those of straight conductors are plotted against conductor length, i.e. number of turns, with closed triangles and open reverse triangles, respectively. The coupling time constants of the conductors wound into pancake coils are larger than those of the straight conductors. The former increases more sharply with increasing length than the latter. In this figure, the solid line shows coupling time constant calculated by using equation (11) with a of 2.75 s m^{-2}, which

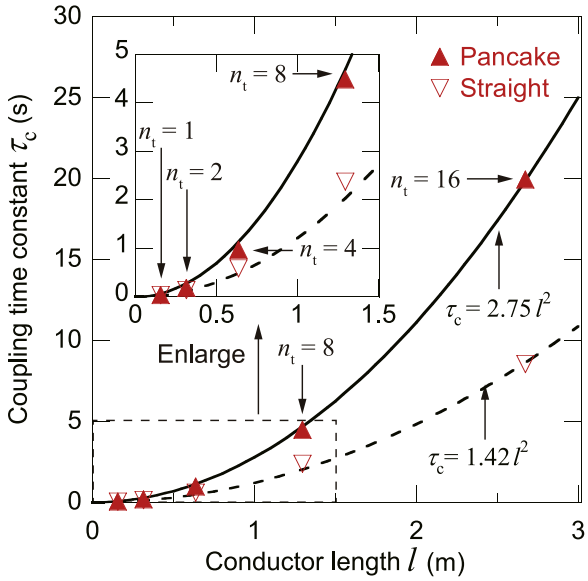

Figure 22. Calculated coupling time constant τ_c of conductors wound into pancake coils with various n_t, i.e. l, (closed symbols) and those of single straight conductors with corresponding l (open symbols) versus l, i.e. n_t. Solid line shows τ_c calculated by using equation (11) with a of 2.75 s m^{-2} obtained from figure 19, which is the value for stacked straight conductors with $n_c = 16$, and the broken line shows τ_c calculated by using equation (11) with a of 1.42 s m^{-2} obtained in figure 19, which is the value for the single straight conductor.

is the value for stacked straight conductors with $n_c = 16$. The broken line shows coupling time constant calculated by using equation (11) with a of 1.42 s m^{-2}, which is the value for the single straight conductor. It should be noted that the coupling time constants of the conductors wound into pancake coils are almost on the solid line when $n_t = 8$ ($l = 1.30$ m) and $n_t = 16$ ($l = 2.67$ m). This suggests that the mutual coupling between the sections of the coupling current path in different turns could be the reason for larger coupling time constant and its sharp increase with increasing length in pancake coils. In other words, equation (11) with a of 2.75 s m^{-2}, which is derived for a 16-stacked straight conductor but not for pancake coils, is reasonably applicable to estimate the coupling time constants of the conductors wound into pancake coils.

5.2. Analytical estimation of coupling time constant of 4 mm wide, four-filament coated conductor wound into pancake coil

Similar to the discussion in the last part of section 5.1, using equation (11) with a of 1.60 s m^{-2}, which is the experimentally determined value for the eight-stacked straight conductors shown in figure 15, we can estimate the coupling time constant of the 4 mm wide, four-filament coated conductor wound into a pancake coil. Here, we consider a pancake coil whose inner radius is 60 mm, d is 0.1 mm, and n_t is 200, i.e. l is 100.3 m. The estimated coupling time constant is 1.61 × 10^4 s (4.5 h), which is not a small value, but we can wait until the decay of the coupling current in some applications.

6. Conclusion

The coupling time constants of striated and copper-plated coated conductors are proportional to the square of the conductor length and increase when they are stacked because of the mutual coupling between coupling currents in stacked conductors. These observations are useful for estimating the coupling time constants of the striated coated conductors wound into pancake coils.

In the striated and copper-plated coated conductors, the plated copper layers dominate the transverse resistances between superconductor filaments. Consequently, the transverse resistance can be uniform along a conductor, and we can increase the transverse resistance, i.e. decrease the coupling time constant, by decreasing the copper thickness or by using a copper alloy. However, the transverse resistance could decrease with decreasing temperature: the coupling time constant could be inversely proportional to the temperature-dependent resistivity of copper.

The striation of coated conductors is effective for reducing the shielding-current-induced field in pancake coils even if they are plated with copper after striation in order to enhance the current sharing. Although the striated coated conductor in a pancake coil is not twisted, the coupling current decays gradually owing to the finite length of the conductor. The increasing number of turns should naturally increase the coupling time constant owing to the increasing conductor length, i.e. increasing self-inductance and decreasing entire transverse resistance of the coupling current path. Moreover, the mutual coupling between the sections of the coupling current path in different turns results in an increase in the coupling time constants. Even if we consider these factors, the coupling time constant of a pancake coil wound with a 100-m-long conductor is 4.5 h, which is not short but might be tolerable in some dc applications.

Acknowledgments

This work was supported in part by the Japan Science and Technology Agency under the Strategic Promotion of Innovative Research and Development (S-innovation) Program and in part by JSPS KAKENHI Grant Number 16H02326.

ORCID iDs

Naoyuki Amemiya https://orcid.org/0000-0002-3000-864X

References

[1] Gu C, Qu T and Han Z 2007 Measurement and calculation of residual magnetic field in a Bi2223/Ag magnet *IEEE Trans. Appl. Supercond.* **17** 2394–7

[2] Hahn S, Bascuñán J, Kim W, Bobrov E, Lee H and Iwasa Y 2008 Field mapping, NMR lineshape, and screening currents induced field analyses for homogeneity improvement in LTS/HTS NMR magnets *IEEE Trans. Appl. Supercond.* **18** 856–9

[3] Amemiya N and Akachi K 2008 Magnetic field generated by shielding current in high T_c superconducting coils for NMR magnets *Supercond. Sci. Technol.* **21** 095001

[4] Koyama Y, Takao T, Yanagisawa Y, Nakagome H, Hamada M, Kiyoshi T, Takahashi M and Maeda H 2009 Towards beyond 1 GHz NMR: mechanism of the long-term drift of screening current-induced magnetic field in a Bi-2223 coil *Physica* C **469** 694–701

[5] Uglietti D, Yanagisawa Y, Maeda H and Kiyoshi T 2010 Measurements of magnetic field induced by screening currents in YBCO solenoid coils *Supercond. Sci. Technol.* **23** 115002

[6] Yanagisawa Y, Kominato Y, Nakagome H, Hu R, Takematsu T, Takao T, Uglietti D, Kiyoshi T, Takahashi M and Maeda H 2011 Magnitude of the screening field for YBCO coils *IEEE Trans. Appl. Supercond.* **21** 1640–3

[7] Kajikawa K and Funaki K 2011 A simple method to eliminate shielding currents for magnetization perpendicular to superconducting tapes wound into coils *Supercond. Sci. Technol.* **24** 125005

[8] Ahn M C, Hahn S and Lee H 2013 3-D field mapping and active shimming of a screening-current-induced field in an HTS coil using harmonic analysis for high-resolution NMR magnets *IEEE Trans. Appl. Supercond.* **23** 4400804

[9] Ueda H *et al* 2014 Measurement and simulation of magnetic field generated by screening currents in HTS coil *IEEE Trans. Appl. Supercond.* **24** 4701505

[10] Amemiya N, Otake H, Sano T, Nakamura T, Ogitsu T, Koyanagi K and Kurusu T 2015 Temporal behaviour of multipole components of the magnetic field in a small dipole magnet wound with coated conductors *Supercond. Sci. Technol.* **28** 035003

[11] Amemiya N, Sogabe Y, Sakashita M, Iwata Y, Noda K, Ogitsu T, Ishii Y and Kurusu T 2016 Magnetisation and field quality of a cosine-theta dipole magnet wound with coated conductors for rotating gantry for hadron cancer therapy *Supercond. Sci. Technol.* **29** 024006

[12] Iwakuma M *et al* 2016 New method for quick decay of shielding current in REBCO superconducting coils *IEEE Trans. Appl. Supercond.* **26** 4403209

[13] Nakazono K, Ueda H, Ishiyama A, Noguchi S, Miyazaki H, Tosaka T, Kurusu T, Nomura S, Urayama S and Fukuyama H 2017 Numerical evaluation on irregular field generated by screening current in high-field REBCO coil for whole-body MRI *IEEE Trans. Appl. Supercond.* **27** 4400405

[14] Noguchi S and Cingoski V 2017 Simulation of screening current reduction effect in REBCO coils by external AC magnetic field *IEEE Trans. Appl. Supercond.* **27** 4701405

[15] Hwang Y J, Hahn S, Lee S, Jang J Y, Han J H, Lee H, Kim J, Yoem H, Yoon Skim K and Ahn M C 2017 A study on mitigation of screening current induced field with a 3-T 100-mm conduction-cooled metallic cladding REBCO magnet *IEEE Trans. Appl. Supercond.* **27** 4701605

[16] Miyazaki H *et al* 2017 Screening-current-induced magnetic field of conduction-cooled HTS magnes wound with REBCO-coated conductors *IEEE Trans. Appl. Supercond.* **27** 4701705

[17] Dilasser G, Fazilleau P and Tixador P 2017 Experimental measurement and numerical simulation of the screening current-induced field decay in a small ReBCO coil *IEEE Trans. Appl. Supercond.* **27** 4900204

[18] Wang L, Wang Q, Liu J, Wang H, Hu X and Chen P 2017 Screening current-induced magnetic field in a noninsulated GdBCO HTS coil for a 24 T all-superconducting magnet *IEEE Trans. Appl. Supercond.* **27** 8200106

[19] Grilli F and Kario A 2016 How filaments can reduce AC losses in HTS coated conductors: a review *Supercond. Sci. Technol.* **29** 083002

[20] Carr W J Jr and Oberly C E 1999 Filamentary YBCO conductors for AC applications *IEEE Trans. Appl. Supercond.* **9** 1475–8

[21] Cobb C B, Barnes P N, Haugan T J, Tolliver J, Lee E, Sumption M, Collings E and Oberly C E 2002 Hysteretic loss reduction in striated YBCO *Physica* C **382** 52–6

[22] Amemiya N, Kasai S, Yoda K, Jiang Z, Levin G A, Barnes P N and Oberly C E 2004 AC loss reduction of YBCO coated conductors by multifilamentary structure *Supercond. Sci. Technol.* **17** 1464–71

[23] Sumption M, Collings E and Barnes P 2005 AC loss in striped (filamentary) YBCO coated conductors leading to designs for highfrequencies and field-sweep amplitudes *Supercond. Sci. Technol.* **18** 122–34

[24] Levin G A, Barnes P N, Amemiya N, Kasai S, Yoda K and Jiang Z 2005 Magnetization losses in multifilament coated superconductors *Appl. Phys. Lett.* **86** 072509

[25] Amemiya N, Yoda K, Kasai S, Jiang Z, Levin G A, Barnes P N and Oberly C E 2005 AC loss characteristics of multifilamentary YBCO coated conductors *IEEE Trans. Appl. Supercond.* **15** 1637–42

[26] Majoros M, Glowacki B A, Campbell A M, Levin G A, Barnes P N and Polak M 2005 AC losses in striated YBCO coated conductors *IEEE Trans. Appl. Supercond.* **15** 2819–22

[27] Barnes P N, Levin G, Varanasi C and Sumption M D 2005 Low AC loss structures in YBCO coated conductors with filamentary current sharing *IEEE Trans. Appl. Supercond.* **15** 2827–30

[28] Kasai S and Amemiya N 2005 Numerical analysis of magnetization loss in finite-length multifilamentary YBCO coated conductors *IEEE Trans. Appl. Supercond.* **15** 2855–8

[29] Levin G A, Barnes P N, Kell J W, Amemiya N, Jiang Z, Yoda K and Kimura F 2006 Multifilament $YBa_2Cu_3O_{6+x}$-coated conductors with minimized coupling losses *Appl. Phys. Lett.* **89** 012506

[30] Suzuki K, Matsuda J, Yoshizumi M, Izumi T, Shiohara Y, Iwakuma M, Ibi A, Miyata S and Yamada Y 2007 Development of a laser scribing process of coated conductors for the reduction of AC losses *Supercond. Sci. Technol.* **20** 822–6

[31] Tsukamoto O and Ciszek M 2007 AC magnetization losses in striated YBCO-123/Hastelloy coated conductors *Supercond. Sci. Technol.* **20** 974–9

[32] Duckworth R C, Paranthaman M P, Bhuiyan M S, List F A and Gouge M J 2007 AC losses in YBCO coated conductor with inkjet filaments *IEEE Trans. Appl. Supercond.* **17** 3159–62

[33] Amemiya N, Kimura F and Ito T 2007 Total AC loss in twisted multifilamentary coated conductors carrying AC transport current in AC transverse magnetic field *IEEE Trans. Appl. Supercond.* **17** 3183–6

[34] Abraimov D, Gurevich A, Polyanskii A, Cai X Y, Xu A, Pamidi S, Larbalestier D and Thieme C L H 2008 Significant reduction of AC losses in YBCO patterned coated conductors with transposed filaments *Supercond. Sci. Technol.* **21** 082004

[35] Marchevsky M, Zhang E, Xie Y, Selvamanickam V and Ganesan P G 2009 AC losses and magnetic coupling in multifilamentary 2G HTS conductors and tape arrays *IEEE Trans. Appl. Supercond.* **19** 3094–7

[36] Šouc J, Gömöry F, Kováč J, Nast R, Jung A, Vojenčiak M, Grilli F and Goldacker W 2013 Low AC loss cable produced from transposed striated CC tapes *Supercond. Sci. Technol.* **26** 075020

[37] Machi T, Nakao K, Kato T, Hirayama T and Tanabe K 2013 Reliable fabrication process for long-length multi-filamentary coated conductors by a laser scribing method for reduction of AC loss *Supercond. Sci. Technol.* **26** 105016

[38] Vojenčiak M, Kario A, Ringsdorf B, Nast R, van der Laan D C, Scheiter J, Jung A, Runtsch B, Gömöry F and Goldacker W 2015 Magnetization AC loss reduction in HTS CORC® cables made of striated coated conductors *Supercond. Sci. Technol.* **28** 104006

[39] Yanagisawa Y, Xu Y, Jin X, Nakagome H and Maeda H 2015 Reduction of screening current-induced magnetic field of REBCO coils by the use of multi-filamentary tapes *IEEE Trans. Appl. Supercond.* **25** 6603705

[40] Demenčík E, Grilli F, Kario A, Nast R, Jung A, Vojenčiak M, Scheiter J and Goldacker W 2015 AC magnetization loss and transverse resistivity of striated YBCO coated conductors *IEEE Trans. Appl. Supercond.* **25** 8201405

[41] Iwakuma M *et al* 2016 Relaxation of shielding current in test coils for MRI With REBCO superconducting scribed tapes *IEEE Trans. Appl. Supercond.* **26** 4401505

[42] Pardo E, Kapolka M, Kováč J, Šouc J, Grilli F and Piqué R N A 2016 Three-dimensional modeling and measurement of coupling AC loss in soldered tapes and striated coated conductors *IEEE Trans. Appl. Supercond.* **26** 4700607

[43] Gyuraki R, Godfrin A, Jung A, Kario A, Nast R, Demencik E, Goldacker W and Grilli F 2016 Interfilament resistance at 77 K in striated HTS coated conductors *IEEE Trans. Appl. Supercond.* **26** 6603606

[44] Iwakuma M, Nabekura K, Yun K, Yoshida K, Sato S, Tomioka A, Konno M, Ibi A, Machi T and Izumi T 2017 Scribing effect on shielding current in REBCO superconducting coils *IEEE Trans. Appl. Supercond.* **27** 4700806

[45] Fujita S *et al* 2017 Characterization of multifilamentary REBCO coated conductor coil fabricated by using the process of scratching the IBAD-MgO layer *IEEE Trans. Appl. Supercond.* **27** 6600504

[46] Willson M 1983 *Superconducting Magnets* (Oxford: Clarendon) pp 174–81

[47] Funaki K and Sumiyoshi F 1995 *Tashinsen to doutai* (Tokyo: Sangyo Tosho) pp 34–5 (*in Japanese*)

[48] Jiang Z and Amemiya N 2004 An experimental method for total AC loss measurement of high T_c superconductors *Supercond. Sci. Technol.* **17** 371–9

[49] Komeda T, Amemiya N, Tsukamoto T, Nakamura T, Jiang Z, Badcock R A, Bumby C, Long N J, Staines M and Buckley R G 2014 Experimental comparison of AC loss in REBCO Roebel cables consisting of six strands and ten strands *IEEE Trans. Appl. Supercond.* **24** 8200505

[50] Nii M, Amemiya N and Nakamura T 2012 Three-dimensional model for numerical electromagnetic field analyses of coated superconductors and its application to Roebel cables *Supercond. Sci. Technol.* **25** 095011

[51] Amemiya N, Tsukamoto T, Nii M, Komeda T, Nakamura T and Jiang Z 2014 Alternating current loss characteristics of a Roebel cable consisting of coated conductors and a three-dimensional structure *Supercond. Sci. Technol.* **27** 035007

[52] Ichiki Y and Ohsaki H 2004 Numerical analysis of AC losses in YBCO coated conductor in external magnetic field *Physica* C **412–414** 1015–20

[53] Amemiya N, Miyamoto K, Banno N and Tsukamoto O 1997 Numerical analysis of AC losses in high-T_c superconductors based on E–J characteristics represented with n-value *IEEE Trans. Appl. Supercond.* **7** 2110–3

[54] Amemiya N, Murasawa S, Banno N and Miyamoto K 1998 Numerical modelings of superconducting wires for AC loss calculations *Physica* C **310** 16–29

[55] Kim Y, Hempstead C and Strnad A 1962 Critical persistent currents in hard superconductors *Phys. Rev. Lett.* **9** 306–9